

Demethylation-induced overexpression of Shc3 drives c-Raf-independent activation of MEK/ERK in HCC

Short Title: Shc3/MVP/MEK/ERK promotes HCC progress

Yun Liu,¹ Xinran Zhang,¹ Baicai Yang,¹ Hao Zhuang,^{1,2} Hua Guo,¹ Wen Wei,³ Yuan Li,⁴ Ruibing Chen,¹ Yongmei Li,^{1*} and Ning Zhang^{1*}

¹ Key Laboratory of Breast Cancer Prevention and Therapy, Laboratory of Cancer Cell Biology, Tianjin Medical University Cancer Institute and Hospital; Research Center of Basic Medical Sciences; Department of Pathogen Biology, School of Basic Medical Sciences; Tianjin Medical University, Tianjin, China.

² Department of Hepatic Biliary Pancreatic Surgery, Cancer Hospital Affiliated to Zhengzhou University, 127 Dongming Road, Zhengzhou, Henan Province, China.

³ School of Life Sciences, Chongqing University, Chongqing, China.

⁴ Department of Laboratory Animal Sciences, Tianjin Medical University.

Keywords: metastasis, proliferation, methylation, microarray

Acknowledgments:

This work was supported by 863 Program (2015AA020403), National Key Research and Development Program (2016YFC0900100), Natural Science Foundation of China (31671421, 81472683, 81602724, 21575103), NSFC-FRQS Program (81661128009), National Key Scientific Instrument and Equipment Development Project (2013YQ16055106). And Postdoctoral Science Foundation of China (2015M580211).

Abbreviations:

HCC, hepatocellular carcinoma; MVP, major vault protein; MEK1/2, mitogen-activated extracellular signal-regulated kinase 1/2; ERK1/2, extracellular signal-regulated kinase 1/2; Shc, Src homolog and collagen homolog; Grb2, growth factor receptor-bound protein 2; PI3K, phosphatidylinositol 3-kinase; kDa, kilodaltons; Gab1, Grb2-associated binding protein 1; ALK, naplastic lymphoma kinase; MAPK, mitogen-activated protein kinase; gDNA, Genomic DNA; ChIP, chromatin immunoprecipitation; qRT-PCR, quantitative reverse transcription PCR; AJCC, American Joint Committee on Cancer; IP, immunoprecipitation; MS, mass spectrometry; Co-IP, co-immunoprecipitation; EGF, epidermal growth factor; EMT, epithelial to mesenchymal transition; 5-aza, 5-aza-2'-deoxycytidine.

Correspondence:

Ning Zhang, Tianjin Medical University, Research Center of Basic Medical Sciences and Cancer Institute and Hospital, Tianjin, 300060, China. E-mail: zhangning@tmu.edu.cn. Phone: +86-13502179648; Fax: 86-22-83336531.

OR

Yongmei Li, Department of Pathogen Biology, School of Basic Medical Sciences, Tianjin Medical University, Tianjin, 300070, China. E-mail: liym@tmu.edu.cn. Phone: +86-13012277187; Fax: 86-22-83336816.

Disclosures: The authors disclose no potential conflicts.

Transcript Profiling: Microarray data have been deposited in the NCBI (GEO

accessions: GSE97626).

Writing Assistance: Springer Nature Author Services and Accdon-LetPub were chosen for the writing assistance.

Abstract

Invasion and intrahepatic metastasis are major factors of poor prognosis in patients with hepatocellular carcinoma (HCC). In this study, we show that increased Src homolog and collagen homolog 3 (Shc3) expression in malignant HCC cell lines associate with HCC invasion and metastasis. Shc3 was significantly upregulated in tumors of 33 HCC patient samples as compared to adjacent normal tissues. Further analysis of 52 HCC patient samples showed that Shc3 expression correlated with microvascular invasion, cancer staging, and poor prognosis. Shc3 interacted with major vault protein (MVP), resulting in activation of MEK1/2 and ERK1/2 independently of Shc1 and c-Raf; this interaction consequently induced epithelial-mesenchymal transition (EMT) and promoted HCC cell proliferation and metastasis. The observed increase in Shc3 levels was due to demethylation of its upstream promoter, which allowed c-Jun binding. In turn, Shc3 expression promoted c-Jun phosphorylation in a positive feedback loop. Analysis of metastasis using a tumor xenograft mouse model further confirmed the role of Shc3 *in vivo*. Taken together, our results indicate the importance of Shc3 in HCC progression and identify Shc3 as a novel biomarker and potential therapeutic target in HCC.

Introduction

Liver cancer is the second leading cause of cancer deaths worldwide (1). The activation of the Ras-extracellular signal-regulated kinase (ERK) pathway, associated with poor prognosis, is detected in nearly half of early HCC patients and almost all advanced HCC patients (2,3). The only available drug for HCC is sorafenib, a small-molecule inhibitor for receptor tyrosine kinases and Raf that shows modest efficacy (4). Thus, there is an urgent need to identify novel drug targets and to develop novel HCC therapies.

One of the key mediators of ERK activation is *Src homolog and collagen homolog 1* (Shc1) (5). Shc1 belongs to a family of adaptor proteins consisting of four members, Shc1, Shc2, Shc3, and Shc4. While Shc1 is ubiquitously expressed in most organs, it is not found in the adult neural system. Shc3, however, is almost exclusively expressed in post-mitotic and mature neurons (6). During neuronal development, there is a switch in expression from Shc1 to Shc3. It has been shown that Shc1 is important for embryonic development, while Shc3 is critical for ensuring proper differentiation (6). Extensive studies have demonstrated that aberrant expression of Shc1 plays a role in malignant transformation, including transformation that leads to HCC (7–11). However, studies and reports on Shc3 in cancers have been limited to studies of aggressive neuroblastomas, high-grade gliomas, and thyroid carcinomas (12–14). Shc3 downregulation impairs neuroblastoma proliferation and significantly inhibits neuroblastoma tumorigenesis in nude mice (12). The function and regulatory mechanism of Shc3 in HCC are largely unknown.

The signal transduction pathways of the Shc proteins have diverse output characteristics. The function and mechanism of action of Shc1 have been studied extensively. Shc1 acts preferentially in the recruitment of growth factor receptor-

bound protein 2 (Grb2), which in turn activates the ERK and/or phosphatidylinositol-4, 5-bisphosphate 3-kinase (PI3K) and Akt pathway. This signaling thereby promotes cell proliferation and survival (8, 15). Moreover, Shc1 has Grb2-independent functions through its binding to other partners, such as the SgK269 pseudokinase, the Arf GTPase activator Asap1, and Ptpn12 phosphatase, to regulate cytoskeletal organization and cell migration (8). In contrast, Shc3 binds to Grb2 with low affinity and activates the ERK pathway less efficiently than Shc1 in neuronal cells (16). In papillary thyroid carcinoma cells, the interaction of Shc3 with Grb2-associated binding protein 1 (Gab1) recruits the p85 subunit of PI3K and activates its downstream effector Akt (17). Therefore, it has been proposed that Shc3 mediates signal transduction through a different molecular mechanism than that used by Shc1 (12).

The Shc3 protein has two isoforms of different sizes: 64 kDa and 52 kDa. In this study, we found increased p64Shc3 expression in highly malignant HCC cell lines using a microarray-based analysis. We further confirmed this finding with our analysis of patient samples. We also identified a novel interaction between p64Shc3 and major vault protein (MVP) and further investigated their mechanism of action and function at both the cellular and organismal levels.

Materials and Methods

Cell lines

HL-7702 cells was originally obtained from the Cell Bank of Shanghai Institutes for Biological Sciences, Chinese Academy of Sciences (Shanghai, China) in 2006 at the passage 25. Hep3B, HepG2, and HEK293T cells were purchased from the American Type Culture Collection biobank within the past 10 years. Huh7 was purchased

from the Japanese Collection of Research Biosources. MHCC97L, MHCC97H, and HCCLM3 cells were obtained from Prof. Zhaoyou Tang. All cells were maintained in media supplemented with 10% FBS, 100 µg/ml streptomycin, and 100 U/ml penicillin. All experiments used early-passage cells and were performed within 1 month after cell thawing. HL-7702, Hep3B, HepG2, HEK293T, and Huh7 cells were authenticated in July 2017. The short tandem repeat analysis were conducted on DNA purified from above cell lines using STR Multi-amplification Kit (MicroreadTM21 ID System) and GeneMapper3.2 software were used to analyze the data. The results were compared with the ATCC and DSMZ databases for reference matching. Also all the cells were negative with EZ-PCR Mycoplasma Test Kit testing (BI, Israel).

Clinical Specimens

Fresh tumor and para-tumor tissues from 33 HCC patients were collected from November 2015 to April 2016 for quantitative reverse-transcription polymerase chain reaction analysis (qRT-PCR, Supplemental Table S1). The relative expression of Shc3 ($2^{-\Delta\Delta Ct}$) was normalized to the endogenous 18S rRNA reference (ΔCt) and related to the median amount of Shc3 in para-tumor tissues. Tumor and para-tumor tissues from 52 HCC patients collected between 2012 and 2015 were embedded in paraffin and were used for immunohistochemistry. Clinical data collection and postoperative follow-up procedures, performed according to a uniform guideline, are also recorded in Supplemental Table S2. Fresh five paired HCC tissue samples were collected from November 2015 to December 2015 for DNA methylation analysis (Supplemental Table S3). All the human liver tissues were obtained from surgically resected samples from HCC patients in Tianjin Medical University Cancer Institute

and Hospital (Tianjin, China). Written informed consent was obtained from all participants in accordance with the Declaration of Helsinki. All experiments were approved by the Ethics Committees of Tianjin Medical University (TMUhMEC2015009, Tianjin, China).

Plasmids and transfection

Expression plasmids of p64Shc3, CH1-Shc3, PTB-Shc3, SH2-Shc3, FLAG-Shc3, and GFP-MVP were constructed to pCDH lentivector (System Biosciences, Palo Alto, CA). The primer sequences used for cloning are listed in Supplemental Table S4. Recombinant genes coding short hairpin RNAs (shRNAs) against Shc3 were constructed to pLKO.1-TRC cloning vector (Addgene, Cambridge, MA, USA). The details of constructions of expression plasmids or shRNA are described in Supplemental Materials and Methods (for shRNA sequences, see Supplemental Table S5). MVP-siRNA duplexes and non-target siRNA were designed and synthesized by RiboBio (Guangzhou, China), and the sequences were listed in Supplemental Table S6. Transient Transfections were performed using Lipofectamine 3000 (Life Technologies, Paisley, Scotland). The primer sequences for qPCR were listed in Supplemental Table S7).

Co-immunoprecipitation

Cell lysates were prepared by incubating cells in 1% Tris-Triton cell lysis buffer (Cell Signaling Technology) containing 1 mM PMSF on ice for 30 min before centrifugation at 12 000 × g for 15 min. The supernatants were incubated overnight with 30 µl of Dynabeads Protein A or Dynabeads Protein G (Life Technologies, Carlsbad, CA, USA) precoated with anti-Shc3, anti-GFP, anti-MEK1/2, anti-MEK1/2

(Santa Cruz, TX, USA), anti-MVP (Abcam, Cambridge, MA, USA), or anti-FLAG (Sigma) antibodies. The immunocomplexes were analyzed by LC-MS/MS analysis or Western blot. A normal IgG control was assayed simultaneously. The details of LC-MS/MS analysis or Western blot are described in Supplemental Materials and Methods.

Gel-filtration analysis

2mg of HCCLM3 cell lysate was separated on a HiPrep 16/60 Sephacryl S-200 HR column (GE, USA) in 50 mM sodium phosphate and 150 mM sodium chloride (pH 7.2). Fractions were analyzed by Western blot.

Cell proliferation assays

Growth curve assay was conducted according to the Kratzat's method (19). Cells were plated in 6-well plates at 5×10^4 /ml density. At each time point, cells were counted and replated at the same density of the start point.

Cell Counting Kit-8 (Dojindo Laboratories, Kumamoto, Japan) was used according to the manufacturer's recommended instruction. Briefly, cells were cultured in 96-well plates. 10 μ l of CCK-8 reagent and 90 μ l of complete culture medium were mixed and added to each well. The absorbance was measured at 450 nm after 3 hours of incubation at 37°C.

For colony formation assay, 10^3 cells were seeded evenly in 6-well plates and medium was changed every 3 days. After two weeks, cell colonies were stained by 0.01% crystal violet and counted.

Chemotactic, invasion, and wound healing assays

Chemotaxis assays were performed by using micro-Boyden chambers as described previously (20). After cells were incubated with 10ng/ml EGF at 37°C for 8 hours (for Huh7 cells), 6 hours (for HepG2 cells) or 5 hours (for HCCLM3 cells), the membranes were fixed and stained. The numbers of migrating cells were counted by light microscopy at 400×.

Invasion assay was performed using Matrigel-coated transwell chambers (Millipore, Billerica, MA, USA) containing polycarbonate membranes with 8 µm pores. 5×10^4 of pre-starved cells were resuspended in the DMEM and added to the upper chamber. 600 µl of the DMEM was added to the lower chamber with or without 10 ng/ml EGF. After incubated for 24 hours at 37°C, the invading cells on the under surface were fixed, stained, and photographed 6 random regions at 400×.

In wound healing assay, cells were seeded in 6-well plates and grown until 80-90% confluence. The cells were scratched with a pipette tip in the middle of the plate , washed with PBS to remove the detached cells and incubated in a medium containing 1% FBS. The wound closure was monitored microscopically at different time-points and photographed at 0 and 24 hours respectively.

DNA Methylation Analysis

Genomic DNA (gDNA) was extracted from cells using a TIANGEN Genomic DNA Kit (TIANGEN, Beijing, China) according to the manufacturer's recommended protocols. Bisulfite modification of the gDNA was performed based on Herman's method (21). HCC tissue samples were subjected to the same procedures as performed with the cell lines. Specific procedures are detailed in the Supplemental Materials and Methods and primer sequences were listed in Supplemental Table S8.

In vivo metastasis assays

An *in vivo* xenograft model was established with 4-week-old male BALB/c-nude mice (Aoyide laboratory animal technology, Tianjin, China), which were injected subcutaneously with 5×10^6 cells into the right thigh region of the animals ($n = 5$ for each cell line). An orthotopic mouse model was inoculated with 1×10^6 cells/mice in the left hepatic lobe of 4-week-old male BALB/c-nude mice ($n = 3$ for each cell line). The specific procedure is detailed in the supplemental materials and methods. All animals received human care according to the “Guide for the Care and Use of Laboratory Animals” (http://oacu.od.nih.gov/ac_cbt/guide3.htm) and the experimental protocols were approved by the Institutional Review Board of Tianjin Medical University.

Statistical Analysis

Clinicopathological correlations were analyzed using the Pearson’s *chi-square* test. Differences among three groups or between two groups were assessed by either two-way ANOVA or Student’s *t*-test, respectively. All statistical tests were two-sided, and differences were considered statistically significant for $p < 0.05$. SPSS 22.0 software was used to analyze the data. Biological experiments were repeated at least three independent times.

Results

Increased Shc3 expression is associated with HCC invasiveness. To identify genes that mediate HCC invasion and micro-metastasis, a microarray assay (Gene Expression Omnibus accession ID: GSE97626) was performed on cell lines Huh7, MHCC97L, and HCCLM3 – 3 HCC cell lines with increasing metastatic potential

(22). Shc3 was remarkably upregulated in the malignant HCC cells as compared with the Huh7 cells with MHCC97L at 3.8-fold and HCCLM3 at 4.6-fold expression than that of Huh7 ($p < 0.05$) (Figure 1A). Quantitative reverse transcription PCR (qRT-PCR) and Western blots further confirmed a significant increase in Shc3 in the highly malignant MHCC97L and HCCLM3 cells (Figure 1B and C) as compared to Huh7 cells. Among the four Shc family proteins, Shc3 was the most strongly overexpressed, while the increases in Shc1 and Shc4 expression were modest (Figure 1B). A similar increase in expression was seen for full-length p64Shc3 relative to total Shc3 (Figure 1C, Supplemental Figure S1). Therefore, we chose to investigate the longer isoform, p64Shc3, for our studies herein.

The clinical relevance of Shc3 mRNA expression in 33 paired tumor and para-tumor HCC samples was examined by qRT-PCR. The mRNA levels of Shc3 in HCC tumor tissues and para-tumor tissues were compared. Higher levels of Shc3 were observed in 81.82% (27 of 33) of HCC samples as compared to its corresponding para-tumor tissues (Figure 1D, Supplemental Table S1). We further explored the clinicopathological characteristics of Shc3 in paraffin-embedded samples from 52 additional patients by immunohistochemistry (IHC). Higher expression of Shc3 was detected in 32 of the 52 samples when expression of Shc3 was compared with that of the corresponding para-tumor tissues (Figure 1E). Expression of Shc3 was associated with microvascular invasion ($\chi^2 = 7.715, p = 0.007$), malignant differentiation ($\chi^2 = 5.333, p = 0.029$), advanced American Joint Committee on Cancer (AJCC) stage ($\chi^2 = 3.989, p = 0.042$) (Supplemental Table S2), and shorter overall survival ($\chi^2 = 4.351, p = 0.037$) (Figure 1F). These results suggest that increased expression of Shc3 might play an important role in HCC progression and invasion.

Major vault protein (MVP) serves as a bridge for Shc3 to interact with MEK and ERK. Immunoprecipitation (IP) and mass spectrometry (MS) were performed to identify proteins that interact with Shc3. MS showed that MVP associates with Shc3 (Figure 2A, Supplemental S2A). As shown in Figure 2B, the interaction between Shc3 and MVP was further confirmed by co-IP. IP using a Shc3 antibody pulled down MVP (Figure 2B, left panel). Reciprocally, IP using an MVP antibody pulled down Shc3 (Figure 2B, right panel), but not Shc1 (Supplemental Figure S2B).

Activation of the ERK pathway is often associated with HCC (3), and MVP has been reported to interact with ERK1/2 (23). We also found that MVP co-immunoprecipitated with both MEK1/2 and ERK1/2 in HCCLM3 cells (Supplemental Figure S2B). Thus, we speculated that MVP might serve as a novel adaptor between Shc3 and MEK1/2 or ERK1/2 in HCC cells. To test this hypothesis and to validate the specificity of the interaction between Shc3 and MVP, we co-expressed FLAG-tagged Shc3 and GFP-tagged MVP constructs in 293T cells, in which Shc3 and MVP are both below detection (Supplemental Figure S2C). IP with anti-FLAG antibodies but not control IgG, specifically co-precipitated GFP-tagged MVP, MEK1/2, and ERK1/2 (Figure 2C, left). And IP with anti-GFP antibodies but not control IgG, also co-precipitated FLAG-tagged Shc3, MEK1/2, and ERK1/2 (Figure 2C, right). Furthermore IP with a Shc3 antibody pulled down both MEK1/2 and ERK1/2 but not c-Raf in HCCLM3 cells (Figure 2D, Supplemental Figure S2D). We also determined the stoichiometry of Shc3, MVP, MEK and ERK composition by gel-filtration analysis. In HCCLM3 cells, almost all of the MVP and more than half of the Shc3 and ERK were eluted simultaneously at fraction #36-40, which is indicative of a Shc3, MVP, MEK and ERK complex. The remainder of the Shc3, MEK, and

ERK were eluted at later fractions, correlating with much smaller molecular weights (Figure 2E). Taken together, our results indicate that Shc3, MVP, MEK and ERK form a complex.

To map a specific domain of Shc3 necessary for its interaction with MVP, we constructed truncation vectors of Shc3. The structure of Shc family members is characterized by a central collagen-homology 1 (CH1) domain flanked by a N-terminal phosphotyrosine binding (PTB) domain and a C-terminal Src-homology (SH2) domain (8). PTB or SH2 domain is employed to bridge between receptor tyrosine kinases (RTKs) and transduce phosphotyrosine-dependent signals. CH1 domain provides binding sites for its binding partners such as Grb2 (24). The results from co-IP showed that MVP, MEK1/2 or ERK1/2 co-precipitated with CH1-Shc3 respectively, but not with the other truncation constructs PTB-Shc3 and SH2-Shc3 (Figure 2F). These results indicate that Shc3 interacts with MVP through the CH1 domain of Shc3. Further examination revealed that MVP knockdown impaired the co-IP between Shc3 and MEK1/2 or ERK1/2 (Figure 2G). Taken together, these results suggest that MVP serves as a bridge for Shc3 to interact with MEK and ERK in HCC cells. Furthermore, Shc3, but not Shc1, interacts physically with MVP.

Shc3 and MVP interaction potentiates ERK signaling independent of Shc1 and c-Raf. We sought to examine whether the Shc3 and MVP interaction resulted in activation of MEK and ERK pathway. In the following experiments, Shc3 was stably overexpressed in Huh7 and HepG2 cells or knocked down in HCCLM3 and HepG2 cells (Supplemental Figure S3A). The expression of Shc1, Shc2, and Shc4 were not altered by the overexpression or the knockdown of Shc3 (Supplemental Figure S3B). Western blots showed that Shc3 overexpression induced a significant

increase in the phosphorylation of MEK1/2 and ERK1/2 (Figure 3A, left), whereas Shc3 knockdown impaired their phosphorylation (Figure 3A, right). Interestingly, phosphorylation of c-Raf was only marginally affected upon Shc3 overexpression or knockdown (Figure 3A). Although it has been reported that Shc3 activates the PI3K-Akt pathway in neuronal and thyroid carcinoma cells (17, 25), we did not find an increase in activated Akt in response to the Shc3 overexpression in HCC cells (Supplemental Figure S3C).

In addition, we investigated the role of MVP in Shc3 potentiated MEK and ERK phosphorylation. Shc3 overexpression increased phosphorylation of MEK and ERK, which was further enhanced by EGF treatments (Figure 3B). Knockdown of MVP significantly impaired phosphorylation of ERK induced by overexpression of Shc3 (Figure 3B, Supplemental Figure S3D). Knockdown of MVP also inhibited EGF-induced phosphorylation of MEK and ERK (Figure 3B). However, EGF-induced phosphorylation of c-Raf was not altered by MVP knockdown. These results suggest that Shc3 and MVP played an important role in EGF-induced activation of MEK and ERK, probably independent of c-Raf activation.

It has been well documented that the Shc1 interaction with Grb2 mediates EGF-induced activation of c-Raf (26). Our results revealed that Grb2 only appeared to bind to Shc1 but not Shc3 in HCCLM3 cells (Supplemental Figure S3E). Thus, we further examined the role of Shc1 and c-Raf in the function of Shc3, MVP, MEK and ERK complex. Knockdown of Shc1 did not interfere with the expression of MVP, Shc3, MEK1/2, or ERK1/2 (Figure 3C). Nor did it disrupt the interaction between Shc3 and MVP, MEK1/2, and ERK1/2 (Figure 3C). As shown in Figure 3D and 3E, overexpression of Shc3 potentiated the phosphorylation of MEK and ERK in the absence of Shc1 or c-Raf. Furthermore, EGF was capable of inducing the

phosphorylation of MEK and ERK in Shc1- or c-Raf-knockdown cells. Therefore, EGF-induced activation of Shc3, MVP, MEK, and ERK complex appeared to be independent of Shc1 and c-Raf pathway. Interestingly, knockdown of Shc3 significantly impaired EGF-induced phosphorylation of MEK and ERK, suggesting that Shc3 and MVP might play a dominant role in MEK and ERK activation in comparison to Shc1 and c-Raf in HCCLM3 cells (Supplemental Figure S3F, Figure 3D). However, the importance of Shc3 and MVP as compared to Shc1 and Grb2 in hepatoma needs further investigation.

Taken together, these results suggest a novel mechanism by which Shc3 engages MVP to activate MEK and ERK pathway through direct interaction with MEK and ERK in HCC independent of Shc1 and c-Raf.

MVP and ERK mediate Shc3-dependent HCC proliferation, migration, invasion, and an epithelial-to-mesenchymal transition (EMT) in vitro. It has been reported that ERK activation promotes cell proliferation, migration, and invasion (3). Therefore, we examined the functional significance of Shc3 expression in HCC. Shc3 overexpression enhanced cell proliferation in Huh7 and HepG2 cells, while Shc3 knockdown impaired cell proliferation in HCCLM3 and HepG2 cells (Figure 4A, Supplemental Figure S4A). Next, we investigated the potential roles of Shc3 in migration and invasion. A wound healing assay showed that Shc3 overexpression significantly increased cell migration, whereas Shc3 knockdown decreased cell migration (Figure 4B, Supplemental Figure S4B). In invasion assays, Shc3 overexpression enhanced cell invasion, and Shc3 knockdown inhibited EGF-mediated invasion (Figure 4C, Supplemental Figure S4C). EGF-induced chemotaxis was also enhanced in Shc3-overexpressing cells and impaired in Shc3-knockdown cells (Figure

4D, Supplemental Figure S4D). Taken together, these results indicate that increased Shc3 expression promotes HCC cell proliferation, migration and invasion.

We also noticed altered cell morphology in the Shc3-knockdown cells, suggesting a role for Shc3 in EMT (Supplemental Figure S5A). Consistent with this, mesenchymal markers, including N-cadherin, vimentin, snail, and slug were markedly upregulated in Shc3-overexpressing cells but significantly downregulated in Shc3-knockdown cells at both the RNA and protein levels (Figure 4E and F, Supplemental Figure S5B). Moreover, E-cadherin, an epithelial marker, was substantially decreased in Shc3-overexpressing cells and increased in Shc3-knockdown cells (Figure 4E and F, Supplemental Figure S5B). Immunofluorescence analysis also showed that N-cadherin expression was markedly elevated in Shc3-overexpressing cells and significantly decreased in Shc3-knockdown cells (Supplemental Figure S5C). These observations indicate that Shc3 may play an important role in EMT in HCC cells.

We further examined the role of MVP-mediated ERK activation in Shc3-dependent EMT. Treatment with PD98059, a specific ERK inhibitor, blocked Shc3-mediated expression of mesenchymal biomarkers and restored Shc3-impaired E-cadherin expression (Figure 4G). Moreover, MVP knockdown restored E-cadherin expression and impaired the expressions of mesenchymal markers at both the RNA and protein levels in the Shc3-overexpressing cells to similar levels as compared to the corresponding control cells (Figure 4H and I). In addition, Shc3-overexpressing Huh7 cells transfected with short interfering RNAs targeting MVP (siMVPs) had less proliferation and migration abilities than Shc3-overexpressing Huh7 cells (Supplemental Figure S6A&B). Taken together, these results suggest that MVP and ERK mediate Shc3-mediated proliferation, migration, invasion, and EMT in HCC.

The Shc3 promoter is hypomethylated in malignant HCC cells. We explored the molecular mechanism underlying the increase in Shc3 expression in malignant HCC cells. Genomic DNA sequencing analysis revealed that the promoter region of Shc3 from -1770 to -1164 relative to the transcription start site contained 18 CpG sites (Supplemental Figure S7A). Bisulfite sequencing revealed that the Shc3 promoter region was highly methylated in Huh7 cells and that the average methylation rate was $67.78 \pm 12.23\%$, CpG methylation, however, was rarely detected in MHCC97L and HCCLM3 cells, which could account for the differences in the Shc3 protein expression profiles observed in these 3 cell lines (Figure 5A, 5B, and 1C). Moreover, Shc3 expression was restored in Huh7 cells by treatment with DNA demethylating agent 5-aza-2'-deoxycytidine (5-aza) in a dose-dependent manner (Figure 5C).

In tissue samples from 5 HCC patients, the methylation rates of the Shc3 promoter region in tumor tissues were significantly lower than in the corresponding para-tumor tissues (Figure 5D and E). Analysis of The Cancer Genome Atlas (TCGA) database further confirmed that Shc3 expression negatively correlates with methylation in HCC patients (Pearson's correlation coefficient = -0.35 , $p < 0.0001$, Supplemental Figure S7B). Taken together, demethylation of the Shc3 promoter could cause increased Shc3 expression in HCC.

c-Jun binds to hypomethylated regions of the Shc3 promoter and promotes Shc3 expression. Through a search of the TRANSFAC professional database, we identified c-Jun as a predicted transcription factor that binds to the last CpG site located at -1224 in the Shc3 promoter region. This site was frequently methylated in Huh7 cells and the para-tumor tissues but not in HCCLM3 cells (Figure 5A and D).

In chromatin immunoprecipitation (ChIP) assays, the Shc3 promoter was pulled down in anti-c-Jun IP assays in HCCLM3 cells but not in Huh7 cells, suggesting that c-Jun binds to the demethylated Shc3 promoter (Figure 6A). Treatment of Huh7 cells with 5-aza enhanced binding between c-Jun and the Shc3 promoter in a dose-dependent manner (Figure 6B).

Furthermore, we transiently transfected a c-Jun expression plasmid into HCCLM3 and Huh7 cells. The overexpression of c-Jun increased expression of Shc3 in HCCLM3 cells but had little effect on Shc3 expression in Huh7 cells (Figure 6C). Taken together, these data suggest that demethylation of the Shc3 promoter is required for c-Jun binding, which in turn elicits increased expression of Shc3 in malignant HCC cells

Next, we examined the impact of Shc3 expression on c-Jun expression. As shown by confocal fluorescence microscopy, transient overexpression of Shc3 in Huh7 cells increased c-Jun expression, especially in the nucleus (Figure 6D). Western blots showed that Shc3 overexpression increased the total levels of c-Jun and the levels of c-Jun inside the nucleus (Figure 6E). GAPDH was used as a cytosolic marker, and histone H3 was used as a nuclear marker. The active, phosphorylated form of c-Jun was also enriched in the nucleus. Therefore, increased levels of Shc3 appeared to stimulate the expression and activation of c-Jun, resulting in a positive feedback mechanism between Shc3 and c-Jun (Figure 6F).

Shc3 promotes tumor growth and intrahepatic metastasis in vivo. To determine the tumorigenic relevance of Shc3 *in vivo*, we first examined the effects of Shc3 in a subcutaneous xenograft model. In 5 weeks, Shc3-overexpressing cells grew into large tumor masses, whereas Shc3 downregulation significantly reduced the size and

weight of the tumors. These findings suggest that Shc3 plays an important role in tumor progression *in vivo* (Figure 7A and B). IHC staining revealed the correlation between Shc3 and the levels of ERK1/2 phosphorylation and Ki67. ERK1/2 phosphorylation and Ki67 were increased in tumors of mice injected with Shc3-overexpressing Huh7 cells. In contrast, Shc3 knockdown reduced Ki67 expression and inhibited ERK1/2 phosphorylation in tumors of mice injected with Shc3-knockdown HepG2 cells (Figure 7C). Extensive tumor foci were detected in the livers of mice injected with HepG2 control cells, whereas very few metastatic foci were detected in the livers of mice subcutaneously implanted with Shc3-knockdown HepG2 cells (Supplemental Figure S8A). Consistent with this observation, the similar reduction in tumor growth was also observed in mice transplanted with Shc3-knockdown HCCLM3 cells (Supplemental Figure S8B and C).

We further examined the role of Shc3 in micro-metastasis using an intrahepatic tumor implantation mouse model. As shown in Figure 7D, Shc3 knockdown significantly reduced the intrahepatic micro-metastasis of HCCLM3 cells. Moreover, stable knockdown of the MVP gene was performed in Shc3-overexpressing Huh7 cells. The knockdown efficiency of MVP expression was confirmed by Western blot (Supplemental Figure S9A). Then the Shc3-overexpressing Huh7 cells, Shc3-overexpressing Huh7 cells with MVP knockdown, and the corresponding control cells were injected orthotopically in the left hepatic lobe of mouse, respectively. The intrahepatic metastasis rate showed that MVP knockdown significantly reduced the intrahepatic metastasis that was promoted by Shc3 overexpression (Supplemental Figure S9B). The results were consistent with results *in vitro*. We further observed intrahepatic metastasis using immunohistochemistry staining with hematoxylin and eosin (H&E). Less extensive tumor foci were observed in mice injected with the

Shc3-overexpressing and MVP-knockdown Huh7 cells compared to mice injected with Shc3-overexpressing Huh7 cells (Supplemental Figure S9C). These results showed that MVP knockdown could rescue the intrahepatic metastasis responding to Shc3 overexpression. Taken together, our results indicate that increased Shc3 expression promotes tumor growth and intrahepatic metastasis, probably through ERK pathway activation.

Discussion

Our results indicate that Shc3 plays an important role in HCC proliferation and metastasis. Previous studies reported that Shc3 is mainly expressed in mature neurons and undetectable in most tissues, including liver, under physiological conditions. Ectopic expression of Shc3 has been reported in neuroblastomas, high grade gliomas, and thyroid carcinomas (12–14). Our results in the present study showed the expression of Shc3 in HCC cell lines, with its expression levels being associated with the malignancy. Higher expression of Shc3 was associated with microvascular invasiveness, cancer staging, and poor prognosis in HCC patients samples. Functional analysis clearly showed that Shc3 promoted cancer cell proliferation and metastasis at both the cellular and organismal levels. The molecular mechanism of Shc1-mediated signal transduction has been extensively documented (8, 15), while the mechanism of action of Shc3 in cancer cells is largely unknown. We addressed this unknown by using mass spectroscopy to analyze proteins that interact with Shc3. Our results showed that Shc3 binds to MVP and that Shc3 formed a complex of Shc3, MVP, MEK, and ERK in highly malignant HCCLM3 cells. The Shc3 protein-protein interactions are functional in cancer cells (27). MVP has been reported to interact with ERK1/2 and to function as a

signaling scaffold for the ERK pathway in fibroblasts (23). A previous study showed that the MAPK/ERK pathway could be activated by Shc3 upregulation in neuroblastoma cells (28). Here, Shc3 appeared to exert its function through MVP. Overexpression of Shc3 potentiated phosphorylation of MEK and ERK which was disrupted by MVP knockdown. Therefore, our studies revealed a novel Shc3, MVP, MEK and ERK complex which mediated Shc3-dependent activation of MEK and ERK in HCC.

Discovery of this Shc3, MVP, MEK, and ERK complex has important clinical implications. MVP, also named as lung resistance-related protein, is upregulated during malignant transformation as well as in multidrug-resistant cancer cells (29, 30). Increased MVP expression is associated with radiation resistance and chemotherapy failure (31). With regards to HCC cells, MVP is not only a potential diagnostic HCC biomarker but also it mediates resistance to EGFR inhibitor in HCC cells (29). EGFR is associated with liver cancer development and recurrence, and is a rational target for HCC therapy (32, 33). MVP is involved in several molecular mechanisms controlling the resistance of HCC cells to EGFR inhibition. For example, MVP overexpression increased EGFR-independent Akt activation in HCC cells (31). In our study, MVP was identified as a novel Shc3 partner that has a profound impact on Shc3-mediated MEK and ERK pathway activation. In addition, EMT acts as one of determinants of the EGFR-inhibitor resistance in HCC cells (34). We showed that MVP knockdown significantly rescue Shc3-induced EMT competences. Therefore, our results expand the understanding of the mechanisms controlling liver tumor resistance to EGFR inhibition.

Activation of ERK was reported in almost all advanced HCC patients (3). Extensive reports have demonstrated the importance of a classic MEK/ERK

activation pathway mediated by Shc1, Grb2, SOS, Ras, and Raf (5). However, Shc3 doesn't seem to employ this classic pathway. Shc3 does not recruit the Grb2-SOS complex in murine embryonic fibroblasts even with EGF treatment (25). Shc3 has low-affinity for Grb2 binding in PC12 cells (16). Co-IP occurred between Grb2 and Shc1 but not between Grb2 and Shc3. Co-IP occurred between Shc3 and MEK and ERK but not between Shc3 and c-Raf. Thus, this novel Shc3, MVP, MEK, and ERK complex did not seem to crosstalk with Shc1, Grb2, or c-Raf. Moreover, Shc3 knockdown significantly impaired phosphorylation of MEK and ERK while the impact on c-Raf phosphorylation was marginal. This suggests that c-Raf was not a downstream mediator of Shc3. Additionally, knockdown of Shc1 or c-Raf did not block EGF-induced phosphorylation of MEK and ERK in Shc3-overexpressing cells. Therefore, Shc3, MVP, MEK, and ERK signal transduction pathway in HCC is probably not less than the classic pathway.

Several receptor tyrosine kinase inhibitors have been tested on HCC patients and only sorafenib showed modest efficacy. Moreover, only approximate 20% of HCC patients respond to sorafenib treatments (4). Sorafenib is a potent inhibitor for tyrosine kinases and c-Raf. Thus, we speculate that this alternative pathway mediated by Shc3 and MVP may play an important role in sorafenib resistance. Further exploration for detailed mechanisms and clinical significance of Shc3 and MVP interaction is needed.

Herein, we next discovered that a positive feedback loop contributed to the ectopic expression of Shc3. Demethylation of the Shc3 promoter regions was found in malignant MHCC97L cells and HCCLM3 cells, which was consistent with the higher expression levels of Shc3 in these cells as compared to Huh7 cells. The reciprocal relationship between the Shc3 expression and the methylation levels in the

Shc3 promoter region was also found in HCC tissues, strongly implicating DNA demethylation as a driver of increased Shc3 expression. Overexpression of Shc3 potentiated ERK activation. It has been reported that the ERK pathway directly mediates phosphorylation on Ser63/73 of the c-Jun N-terminus in murine fibroblasts (35). In human melanoma, active ERK increases c-Jun mRNA levels and c-Jun stability (36). In our study, Shc3 overexpression induced c-Jun expression and c-Jun enrichment in the nucleus. Phosphorylation of c-Jun at Ser73 was also increased, suggesting an increase in the transcriptional activity of c-Jun. We found that c-Jun bound to demethylated promoter region of Shc3, which further increased Shc3 transcription. We speculate that this positive feedback loop amplifies the Shc3, MVP, MEK, and ERK signaling during HCC progression..

In summary, ectopic expression of Shc3, regulated by promoter demethylation and c-Jun, is associated with HCC progression and invasiveness. Shc3 forms a complex with MVP, MEK, and ERK, which potentiates ERK activation, independent of the classic Shc1, Grb2, SOS, Ras, and Raf pathway. The Shc3-potentiated signaling pathway stimulates a repertoire of downstream tumorigenic responses, including proliferation, migration, invasion, and EMT. These data support the possibility of using Shc3 as a novel biomarker and therapeutic target for HCC.

References

1. Torre LA, Bray F, Siegel RL, et al. Global cancer statistics, 2012, CA Cancer J Clin. 2015;65(2015):87-108.
2. Sun JX, Shi J, Li N, et al. Portal vein tumor thrombus is a bottleneck in the treatment of hepatocellular carcinoma. Cancer Biol Med. 2016; 13(4): 452-458.

3. Ito Y, Sasaki Y, Horimoto M, et al. Activation of mitogen-activated protein kinases/extracellular signal-regulated kinases in human hepatocellular carcinoma. *Hepatology* 1998; 27:951-958
4. Llovet JM, Ricci S, Mazzaferro V, et al. Sorafenib in advanced hepatocellular carcinoma. *N Engl J Med.* 2008; 359:378-390.
5. Yong Zheng, et al. Temporal regulation of EGF signaling networks by the scaffold protein Shc1. *Nature*, 2013, 499, 166-171.
6. Conti L, Sipione S, Magrassi L, et al. Shc signaling in differentiating neural progenitor cells. *Nat Neurosci.* 2001; 4(6): 579-586.
7. Zheng Y, Zhang C, Croucher DR, et al. Temporal regulation of EGF signalling networks by the scaffold protein Shc1. *Nature*. 2013; 499(7457):166-171.
8. Im YK, La Selva R, Gandin V, et al. The ShcA adaptor activates AKT signaling to potentiate breast tumor angiogenesis by stimulating VEGF mRNA translation in a 4E-BP-dependent manner. *Oncogene*. 2015; 34:1729-1735.
9. Veeramani S, Igawa T, Yuan TC, et al. Expression of p66(Shc) protein correlates with proliferation of human prostate cancer cells. *Oncogene*. 2005; 24(48):7203-7212.
10. Lebiedzinska-Arciszewska M, Opara M, Vega-Naredo I, et al. The interplay between p66Shc, reactive oxygen species and cancer cell metabolism. *Eur J Clin Invest.* 2015; 45:25-31.
11. Yoshida S, Kornek M, Ikenaga N, et al. Sublethal heat treatment promotes epithelial-mesenchymal transition and enhances the malignant potential of hepatocellular carcinoma. *Hepatology*. 2013; 58(5): 1667-1680.
12. Miyake I, Ohira M, Nakagawara A, et al. Distinct role of ShcC docking protein in the differentiation of neuroblastoma. *Oncogene*. 2009; 28(5): 662-673.

13. Ortensi B, Osti D, Pellegatta S, et al. Rai is a new regulator of neural progenitor migration and glioblastoma invasion. *Stem Cells*. 2012; 30:817–832.
14. De Falco V, Guarino V, Malorni L, et al. RAI(ShcC/N-Shc)-dependent recruitment of GAB 1 to RET oncoproteins potentiates PI3-K signalling in thyroid tumors. *Oncogene*. 2005; 24(41): 6303-6313.
15. Holgado-Madruga M, Emlet DR, Moscatello DK, et al. Grb2-associated docking protein in EGF- and insulin-receptor signalling. *Nature*. 1996; 379: 560–564.
16. Nakamura T, Komiya M, Gotoh N, et al. Discrimination between phosphotyrosine-mediated signaling properties of conventional and neuronal Shc adapter molecules. *Oncogene*. 2002; 21(1): 22-31.
17. De Falco V, Guarino V, Malorni L, et al. RAI(ShcC/N-Shc)-dependent recruitment of GAB 1 to RET oncoproteins potentiates PI3-K signalling in thyroid tumors. *Oncogene*. 2005; 24(41): 6303-6313.
18. Herman JG, Graff JR, Myöhänen S, et al. Methylation-specific PCR: a novel PCR assay for methylation status of CpG islands. *Proc. Natl. Acad. Sci.* 1996; 93: 9821-9826.
19. Kratzat S, Nikolova V, Miethling C, Hoellein A, Schoeffmann S, Gorka O, et al. Cks1 is required for tumor cell proliferation but not sufficient to induce hematopoietic malignancies. *PLoS One*. 2012; 7: 37433.
20. Hongyan Li, Lei Yang, Hui Fu, Jianshe Yan, Ying Wang, Hua Guo. Association between Gai2 and ELMO1/Dock180 connects chemokine signalling with Rac activation and metastasis. *Nature Communications*. 2013 ; 4, 1706.
21. Herman JG, Graff JR, Myohanen S, Nelkin BD, Baylin SB. Methylation-specific PCR: a novel PCR assay for methylation status of CpG islands. *Proc Natl Acad Sci U S A*. 1996; 93, 9821-9826.

22. Sun FX, Tang ZY, Lui KD, et al. Establishment of a metastatic model of human hepatocellular carcinoma in nude mice via orthotopic implantation of histologically intact tissues. *Int J Cancer*. 1996; 66: 239-243.
23. Kolli S, Zito CI, Mossink MH, et al. The major vault protein is a novel substrate for the tyrosine phosphatase SHP-2 and scaffold protein in epidermal growth factor signaling. *J Biol Chem*. 2004; 279(28): 29374-29385.
24. Schüller AC, Ahmed Z, Levitt JA, et al. Indirect recruitment of the signalling adaptor Shc to the fibroblast growth factor receptor 2 (FGFR2). *Biochem J*. 2008;416:189–199
25. Pelicci G, Troglio F, Bodini A, et al. The neuron-specific Rai (ShcC) adaptor protein inhibits apoptosis by coupling Ret to the phosphatidylinositol 3-kinase/Akt signaling pathway. *Mol Cell Biol*. 2002; 22(20): 7351-7363.
26. Bisson N, James DA, Ivosev G, et al. Selected reaction monitoring mass spectrometry reveals the dynamics of signaling through the GRB2 adaptor. *Nat Biotechnol*. 2011; 29(7): 653- 658.
27. Sagi O, Budovsky A, Wolfson M, et al. ShcC proteins: brain aging and beyond. *Ageing Res Rev*. 2015;19:34-42
28. Miyake I, Hakomori Y, Shinohara A, et al. Activation of anaplastic lymphoma kinase is responsible for hyperphosphorylation of ShcC in neuroblastoma cell lines. *Oncogene*. 2002; 21(38): 5823-5834.
29. Megger DA, Bracht T, Kohl M, et al. Proteomic differences between hepatocellular carcinoma and nontumorous liver tissue investigated by a combined gel-based and label-free quantitative proteomics study. *Mol Cell Proteomics*. 2013; 12(7): 2006-2020.
30. Mossink MH, van Zon A, Scheper RJ , et al. Vaults: a ribonucleoprotein particle

- involved in drug resistance? *Oncogene*. 2003; 22(47):7458-67.
31. Losert A, Lötsch D, Lackner A, et al. The major vault protein mediates resistance to epidermal growth factor receptor inhibition in human hepatoma cells. *Cancer Lett.* 2012; 319(2): 164-172.
32. Kira S, Nakanishi T, Suemori S, et al. Expression of transforming growth factor alpha and epidermal growth factor receptor in human hepatocellular carcinoma. *Liver*. 1997; 17(4):177-82.
33. Lanaya H, Natarajan A, Komposch K, et al. EGFR has a tumour-promoting role in liver macrophages during hepatocellular carcinoma formation. *Nat Cell Biol*. 2014; 16(10):972-7.
34. Fuchs BC, Fujii T, Dorfman JD, et al. Epithelial-to-mesenchymal transition and integrin-linked kinase mediate sensitivity to epidermal growth factor receptor inhibition in human hepatoma cells. *Cancer Res*. 2008; 68(7): 2391 - 2399.
35. Dhillon, AS, S. Hagan, O. Rath, W. Kolch. MAP kinase signalling pathways in cancer. *Oncogene*, 2007, 26: 3279-3290.
36. Lopez-Bergami P, Huang C, Goydos JS, et al. Rewired ERK-JNK signaling pathways in melanoma. *Cancer Cell*. 2007; 11(5): 447-460.

Figure Legends

Figure 1. Increased Shc3 expression is associated with HCC metastasis. (A) Differentially expressed mRNAs in Huh7, MHCC97L, and HCCLM3 cells were detected by microarray. Each sample was analyzed in triplicate. Darker colors indicate higher expression levels. Shc3 is shown in red bold font in the right panel. (B) qRT-PCR analysis of relative expressions of Shc family mRNAs in MHCC97L and HCCLM3 cells as compared to those in Huh7 cells. The data are means ±

standard deviation (SD) of triplicate independent experiments ($n = 4$, * $p < 0.05$, by one-way ANOVA) (C) Western blots of Shc3 expression in HCC cell lines. β -actin was used as a loading control. (D) Shc3 mRNA expression in 33 paired HCC clinical samples. The mRNA levels of Shc3 in HCC tumor tissues and para-tumor tissues were compared using a paired Student's *t*-test, * $p < 0.05$. (E) Representative IHC analysis of Shc3 expression in 52 additional paired HCC clinical samples (magnifications at 100 \times and 200 \times). (F) Kaplan-Meier analysis indicating a correlation between Shc3 overexpression and survival in 52 HCC patients.

Figure 2. Major vault protein (MVP) serves as a bridge for Shc3 to interact with MEK and ERK. (A) Image of an SDS-PAGE gel with silver stain. IP was performed with HCCLM3 cell lysates. Normal IgG was used as a control. (B) Co-IP of endogenous Shc3 and MVP in HCCLM3 cells. (C) Co-IP of FLAG-Shc3, GFP-MVP, MEK1/2, and ERK1/2 in 293T cells co-transfected with expression plasmids encoding FLAG-Shc3 and GFP-MVP. (D) Co-IP of endogenous Shc3, MEK1/2 and ERK1/2 in HCCLM3 cells. (E) Shc3, MVP, MEK, and ERK complex stoichiometry in HCCLM3 cells lysates determined by gel-filtration assay. (F) Schematic diagram of the plasmids encoding FLAG-tagged domains of Shc3 (upper panel). Plasmids encoding FLAG-tagged domains of Shc3 were transfected in HCCLM3 cells. Co-IP of FLAG-tagged domains of Shc3, MVP, MEK1/2, and ERK1/2 in HCCLM3 cells(lower panel). (G) Co-IP of Shc3, MEK1/2, and ERK1/2 in HCCLM3 cells transfected with MVP siRNA.

Figure 3. Shc3 and MVP interaction potentiates ERK signaling activation independent of c-Raf. (A) Western blots of the principal components in the MAPK

pathway in Shc3-overexpressing Huh7 cells and Shc3-knockdown HCCLM3 cells (upper panel). The histogram shows the relative intensities of phosphorylation levels of MEK1/2, ERK1/2, and c-Raf (lower panel). (B) Western blots of the principal components in the MAPK pathway in Shc3-overexpressing Huh7 cells transfected with siMVP in the presence or absence of 10 ng/ml EGF (upper panel). The histogram shows the relative intensities of phosphorylation levels of MEK1/2, ERK1/2, and c-Raf (lower panel). (C and D) Co-IP of Shc3, MVP, MEK1/2, and ERK1/2 in HCCLM3 cells transfected with Shc1 siRNAs (C) or c-Raf siRNAs (D). (E) Western blots of the principal components in the MAPK pathway in Shc3-overexpressing Huh7 cells with or without 10 ng/ml EGF treatment (upper panel). The histogram shows the relative intensities of phosphorylation levels of MEK1/2, ERK1/2, and c-Raf (lower panel). Data represent the means \pm standard error (SE) of triplicate independent experiments (* $p < 0.05$, by Student's *t*-test or one-way ANOVA).

Figure 4. MVP and ERK mediates Shc3-dependent proliferation, migration, invasion, and an EMT of HCC *in vitro*. (A) Growth curve of Shc3-overexpressing and Shc3-knockdown cells. (B) Wound healing assay using Shc3-overexpressing and Shc3-knockdown cells. Representative images at 0 hour and 24 hours are shown. (magnification at 100 \times). (C) Invasion assays with or without 10 ng/ml EGF using Shc3-overexpressing and Shc3-knockdown cells. Representative images of the invading cells in the presence of 10 ng/ml EGF are shown (magnification at 400 \times). Histogram of the numbers of invading cells. (D) Chemotaxis analysis of Shc3-overexpressing and Shc3-knockdown cells with different doses of EGF treatment. (E) mRNA levels of EMT markers measured by qRT-PCR in Shc3-overexpressing and Shc3-knockdown cells. (F) Protein levels of EMT markers measured by

Western blot analysis in Shc3-overexpressing and Shc3-knockdown cells. (G) Western blots of ERK1/2 phosphorylation and EMT markers in Shc3-overexpressing Huh7 cells treated with 10 μ M of PD98059. (H) mRNA levels of EMT markers measured by qRT-PCR in Shc3-overexpressing Huh7 cells transfected with MVP siRNAs. (I) Western blots of EMT markers in Shc3-overexpressing Huh7 cells transfected with MVP siRNAs. Data represent the means \pm SE ($*p < 0.05$, by Student's *t*-test or one-way ANOVA).

Figure 5. DNA methylation abrogates Shc3 transcription. (A) Bisulfite sequencing of the Shc3 promoter region in Huh7, MHCC97L, and HCCLM3 cells (n = 10). Black dot: methylated; white dot: unmethylated. (B) Histogram showing of the methylation rate of the CpG islands in the Shc3 promoter. (C) qRT-PCR of Shc3 expression after treatment with different doses of 5-aza for 96 h. (D, E) Bisulfite sequencing of the Shc3 promoter region in the 5 pairs of HCC clinical samples ($*p < 0.05$ by Kruskal-Wallis *H* test).

Figure 6. c-Jun binds to the demethylated promoter region of Shc3 and promotes Shc3 expression. (A) ChIP-PCR analysis of c-Jun binding to the Shc3 promoter in Huh7 and HCCLM3 cells. Data represent the means \pm SD of triplicate independent analyses ($*p < 0.05$, by Student's *t*-test). (B) ChIP-PCR analysis of c-Jun binding to the Shc3 promoter in Huh7 cells with or without 5-aza treatment for 96 hours (n = 4, respectively). Data represent the means \pm SE of triplicate independent analyses ($*p < 0.05$, by one-way ANOVA). (C) Shc3 and c-Jun in Huh7 and HCCLM3 cells transfected with a c-Jun expression plasmid were examined by qRT-PCR (upper panel, n = 4, Data represent the means \pm SE of triplicate independent analyses ($*p < 0.05$, by

Student's *t*-test) and Western blotting (lower panel). (D) Immunofluorescence analysis of Shc3 and c-Jun in Shc3-overexpressing Huh7 cells and the corresponding control cells. (E) Western blots of ERK1/2, c-Jun, and p-c-Jun (Ser73) expression in the whole cell lysates, the cytoplasm, and the nucleus of Shc3-overexpressing Huh7 cells and the corresponding control cells. (F) Schematic representation of the integrated positive feedback loop in which Shc3, MVP, MEK, and ERK complex contributes to HCC progress.

Figure 7. Shc3 promotes tumor growth and intrahepatic metastasis *in vivo*. (A) Size of the subcutaneous tumor formed by injected Shc3-overexpressing or Shc3-knockdown cells and the corresponding control cells over 5 weeks (5×10^6 cells/mouse, $n = 5$, $**p < 0.01$, by repeated measures ANOVA). The tumor volume (V) was determined by measuring the longitudinal diameter (L) and the transverse diameter (W) and then applying the formula $V = (L \times W^2)/2$. (B) Images of the subcutaneous tumors formed by injected Shc3-overexpressing or Shc3-knockdown cells and the corresponding control cells. Histogram showing the weights of the subcutaneous tumors ($n = 5$, $*p < 0.05$, by Student's *t*-test). (C) Representative IHC images of expressions of Shc3, p-ERK1/2, and Ki67 in subcutaneous tumors. Magnification: 200 \times . (D) Representative images showing the intrahepatic metastases (marked with thin red arrows) and the orthotopic transplanted tumor (marked with bold red arrows) in the orthotopic mouse models transplanted with Shc3-knockdown HCCLM3 cells and the corresponding control cells. The surface tumor nodules were counted and plotted ($n = 3$, $*p < 0.05$, by Student's *t*-test). Representative H&E staining images of the orthotopic transplanted tumor. Magnification at 200 \times .

Fig.1

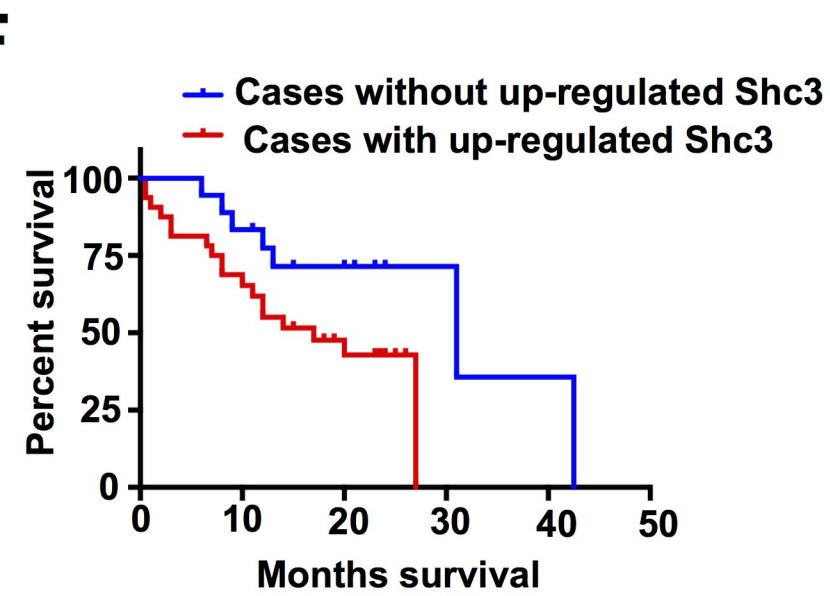
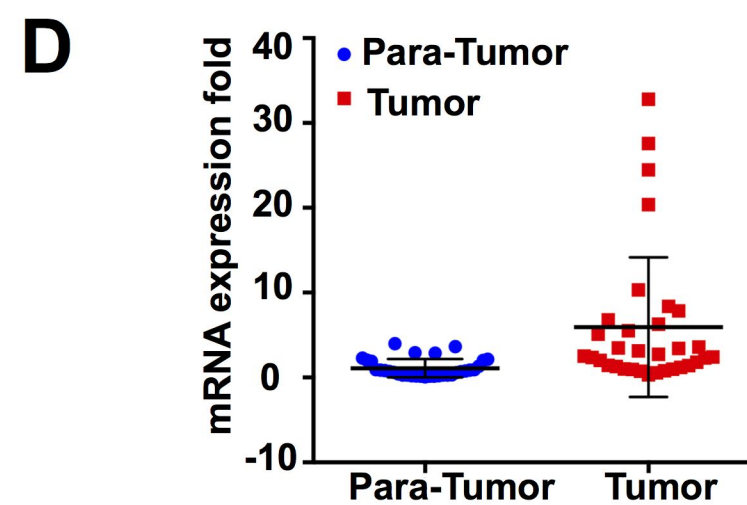
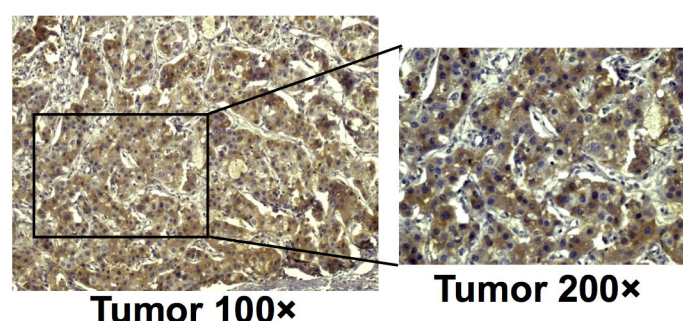
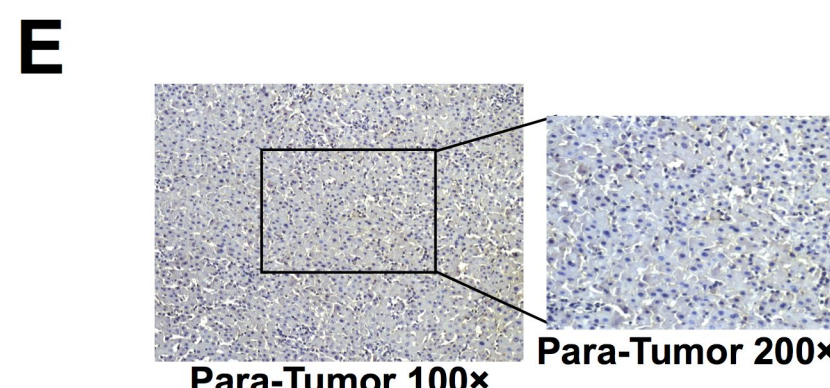
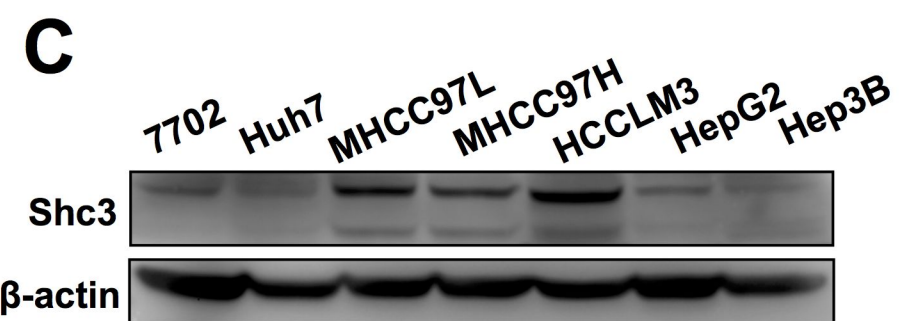
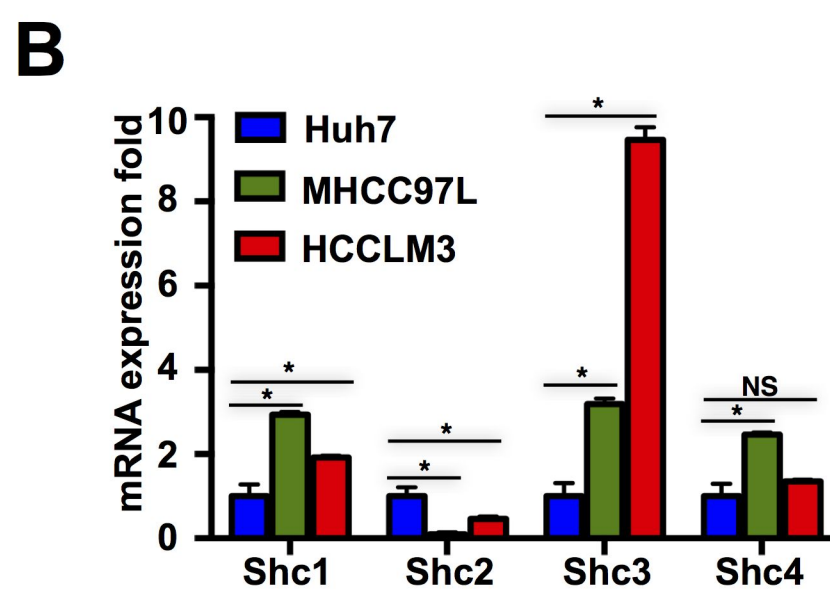
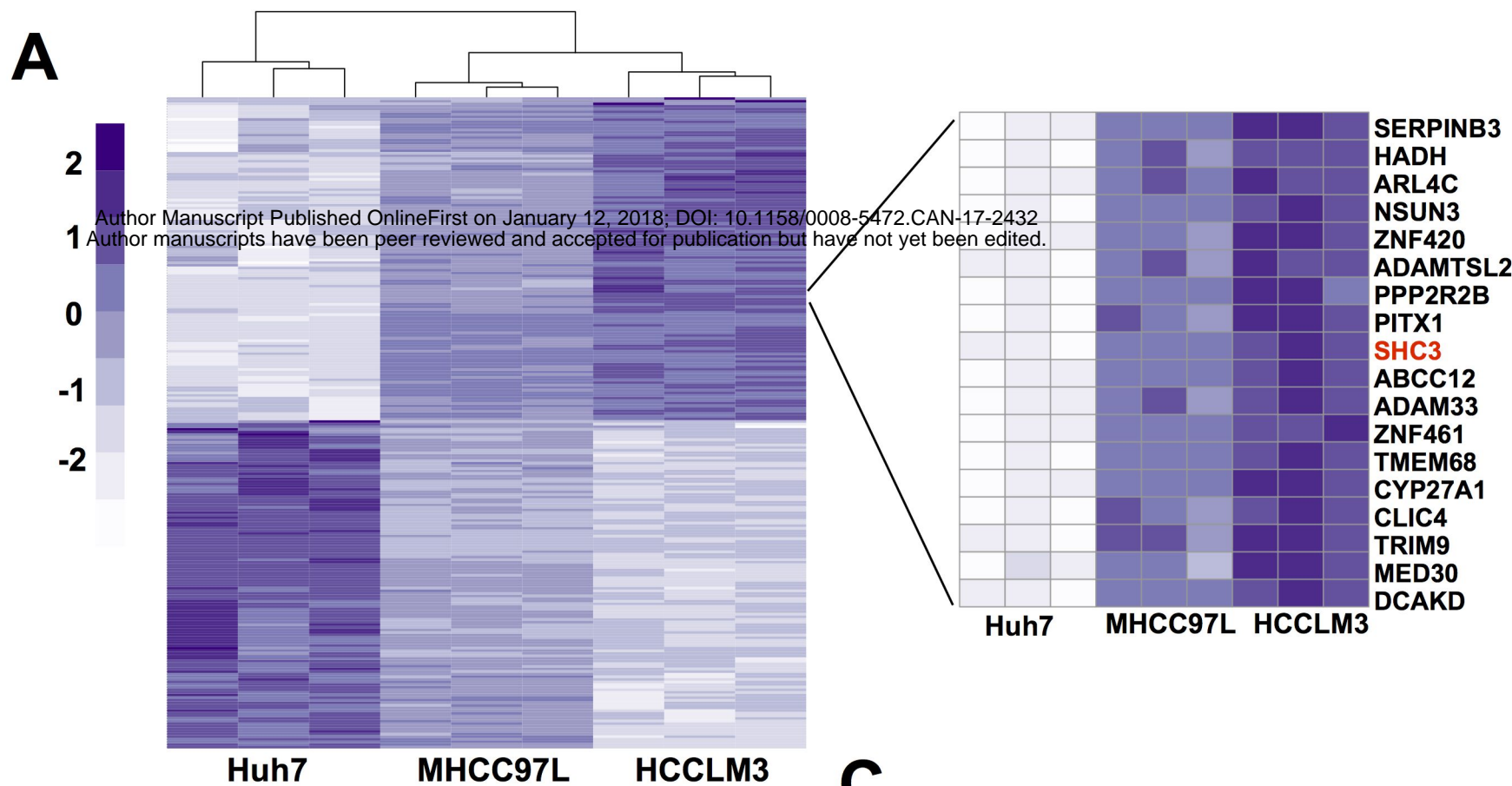


Fig.2

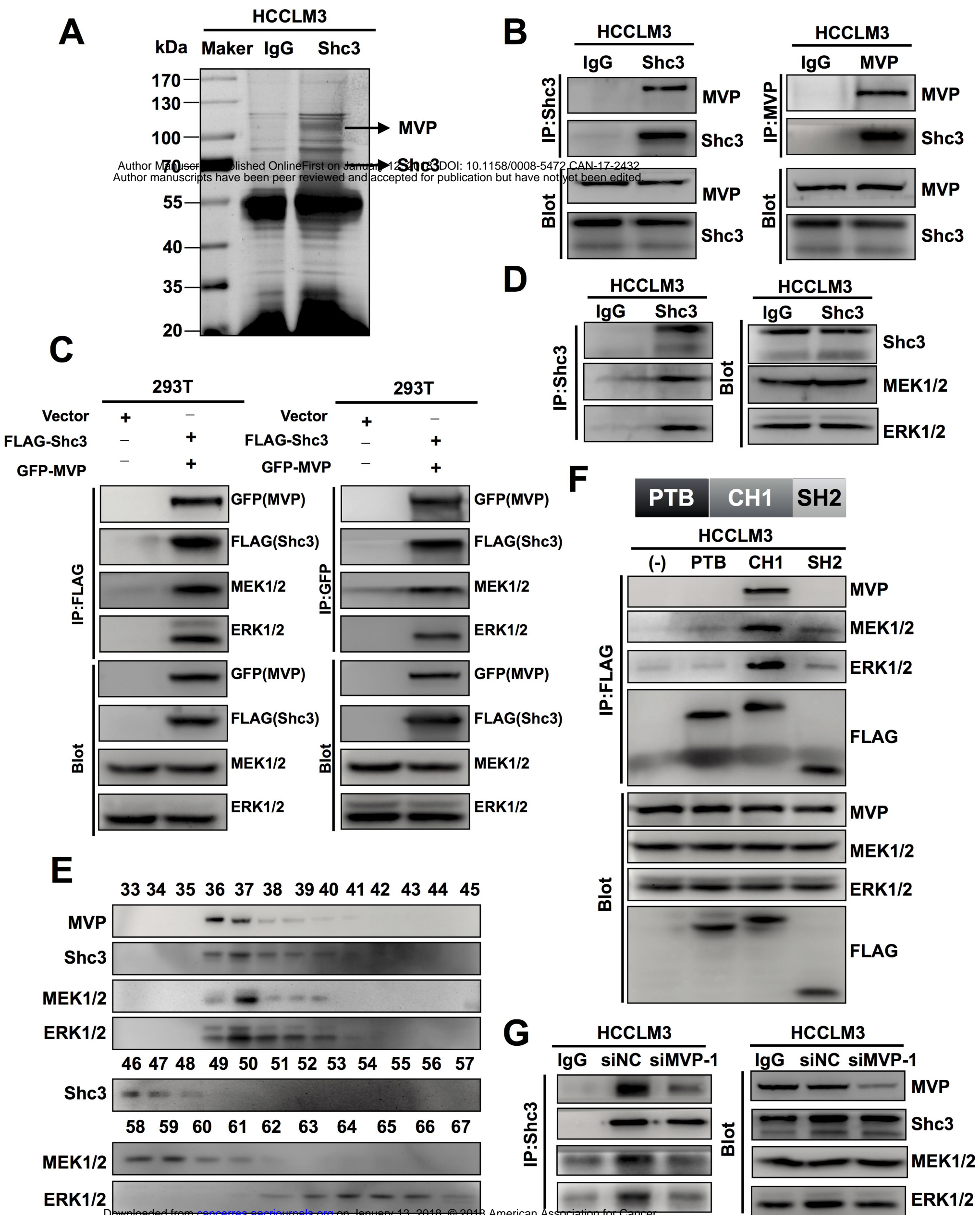
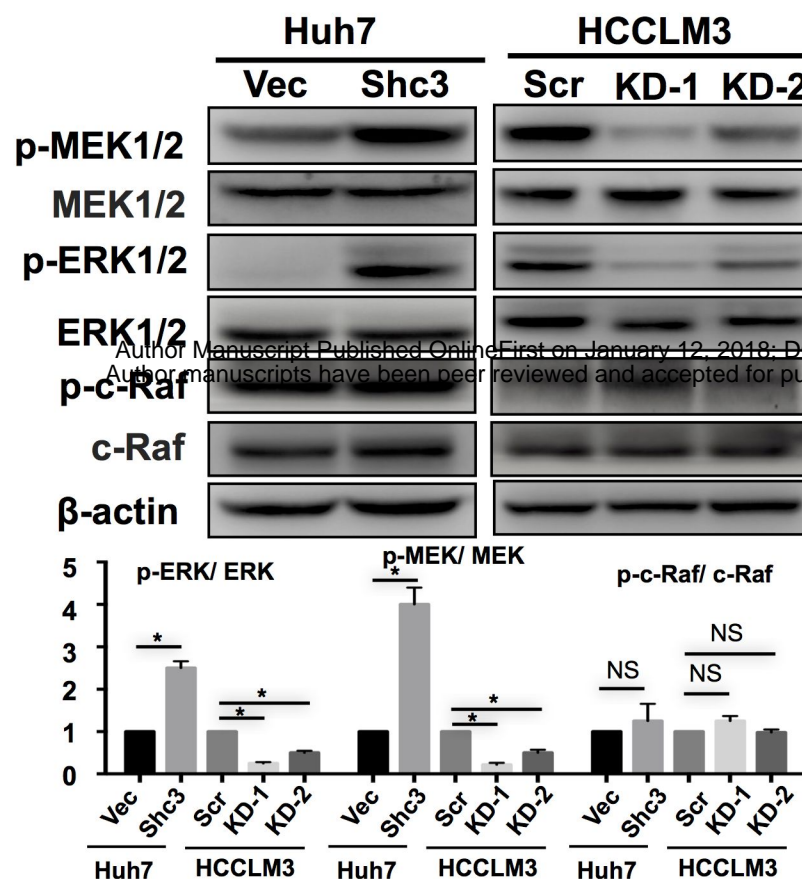


Fig.3**A**

Author Manuscript Published Online First on January 12, 2018; DOI: 10.1158/0008-4542.AN-17-2432
Author manuscripts have been peer reviewed and accepted for publication but have not yet been edited.

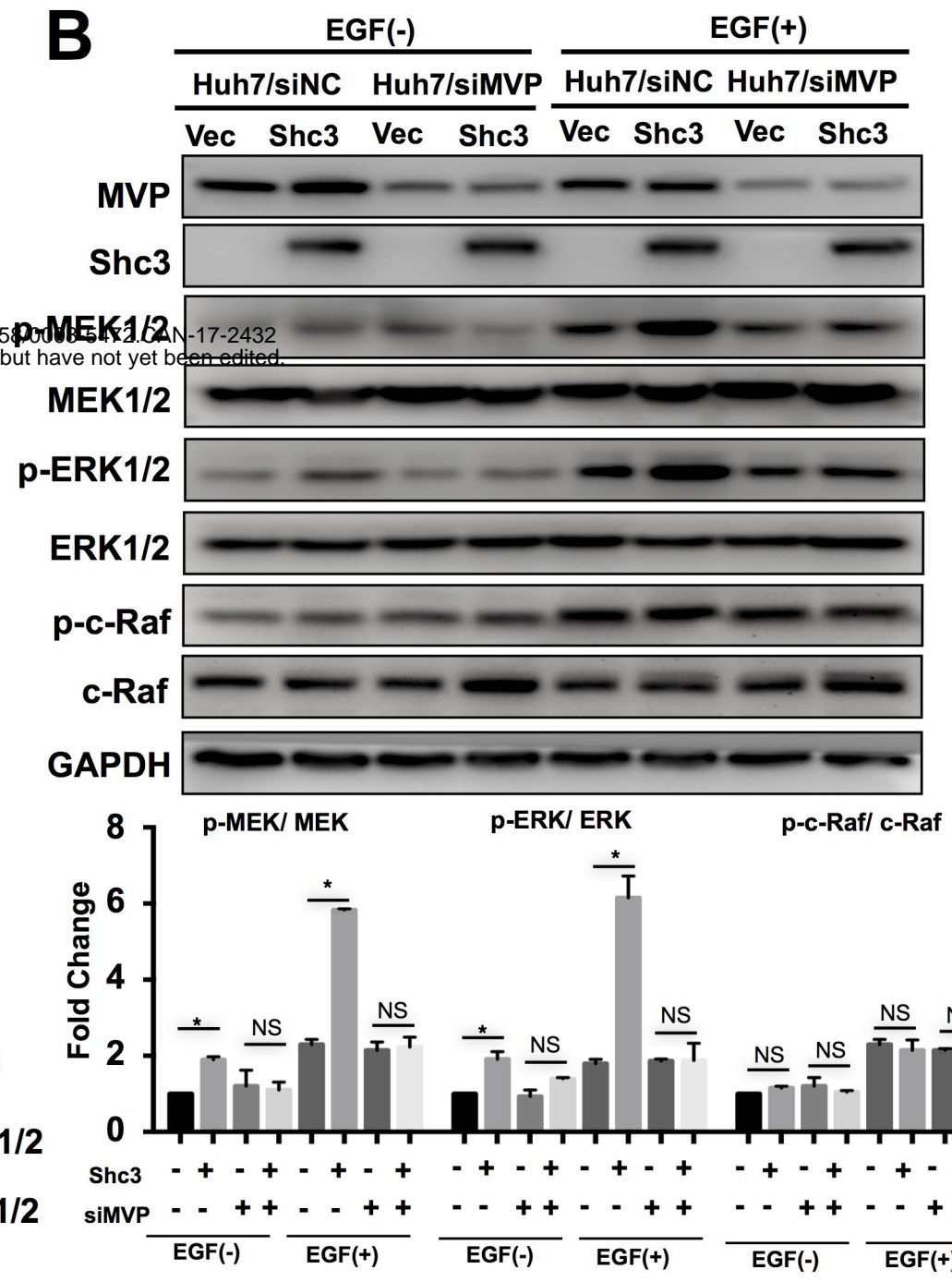
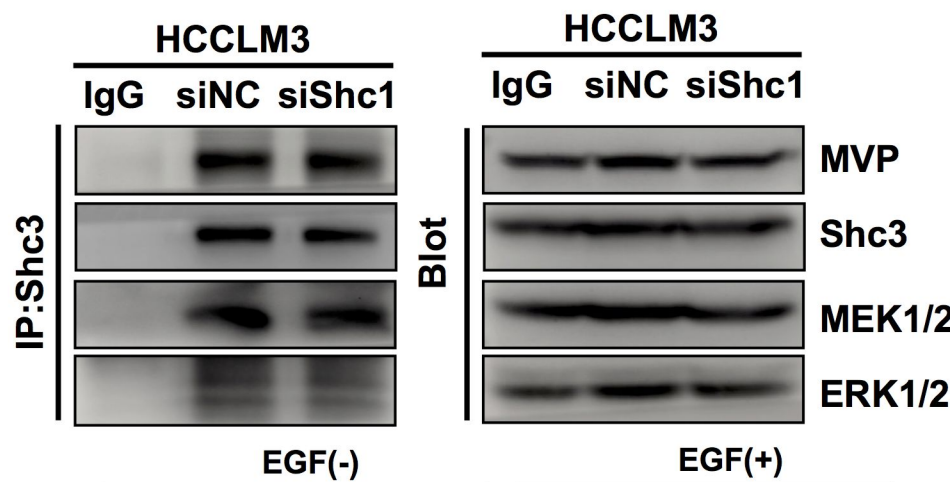
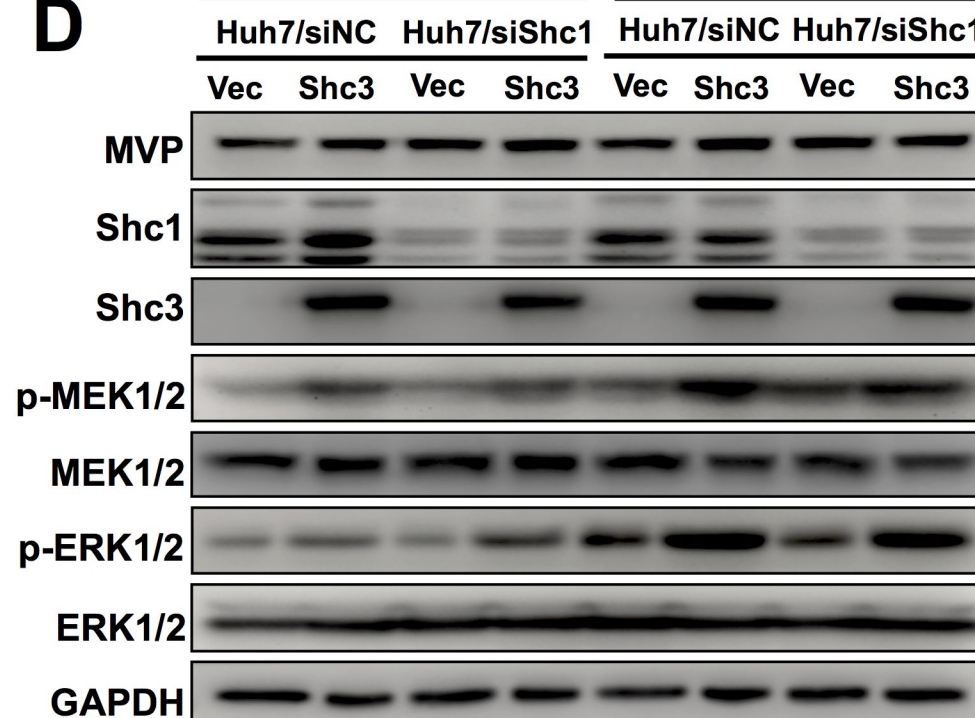
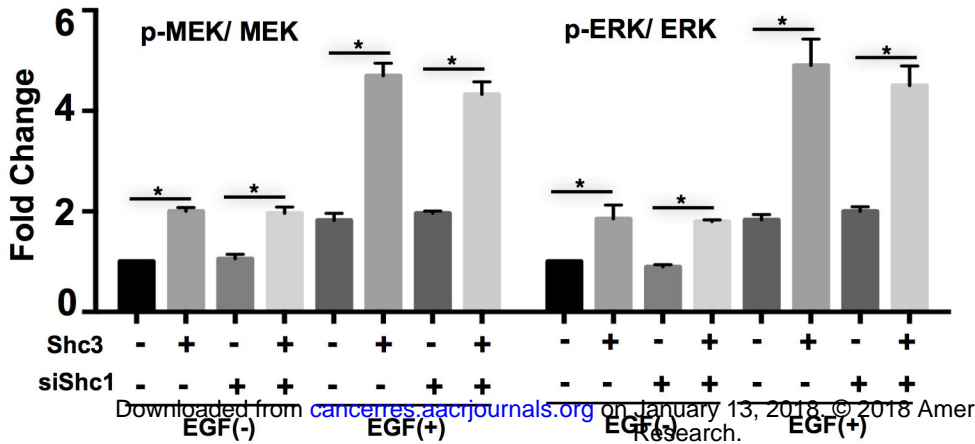
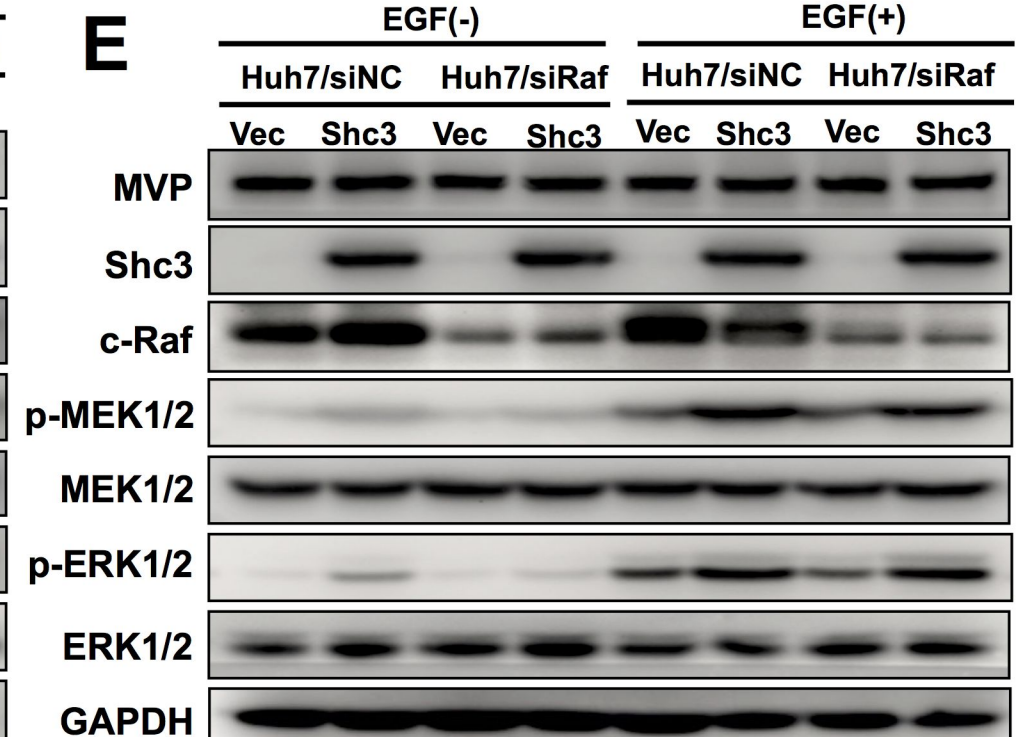
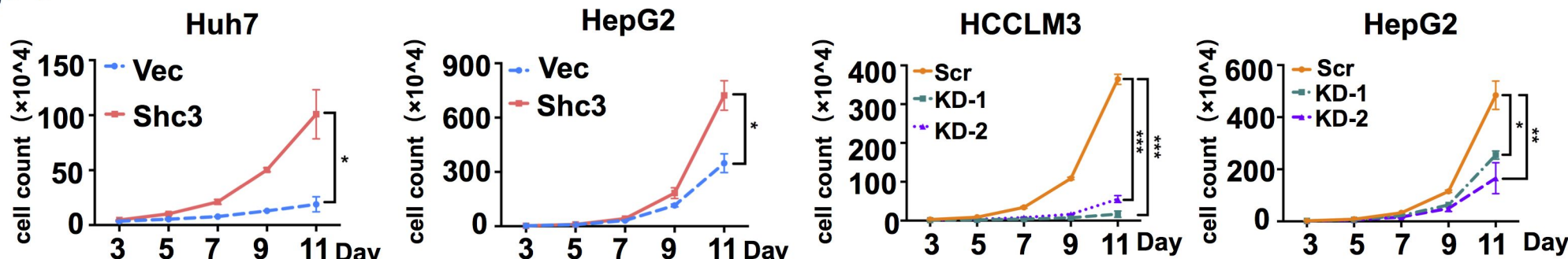
B**C****D****E**

Fig.4**A****B**

Author Manuscript Published OnlineFirst on January 12, 2018; DOI: 10.1158/0008-5472.CAN-17-2432
This author manuscript has been peer reviewed and accepted for publication but have not yet been edited.

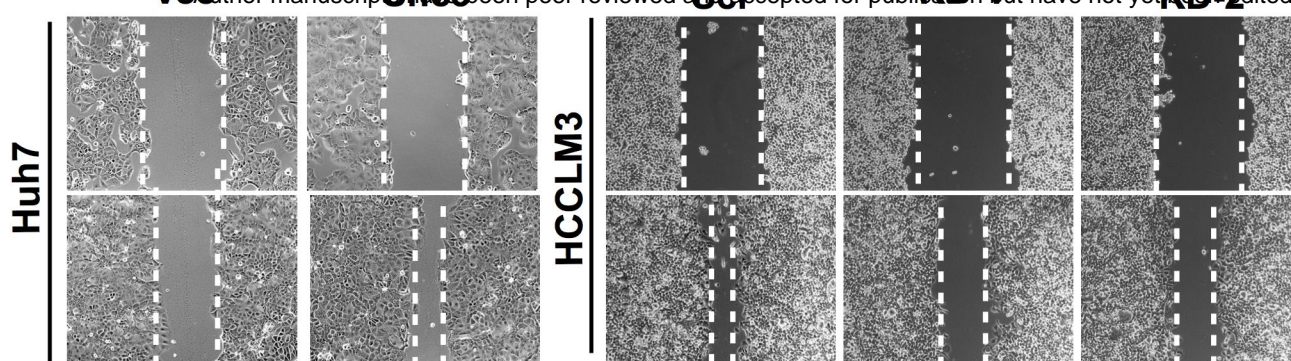
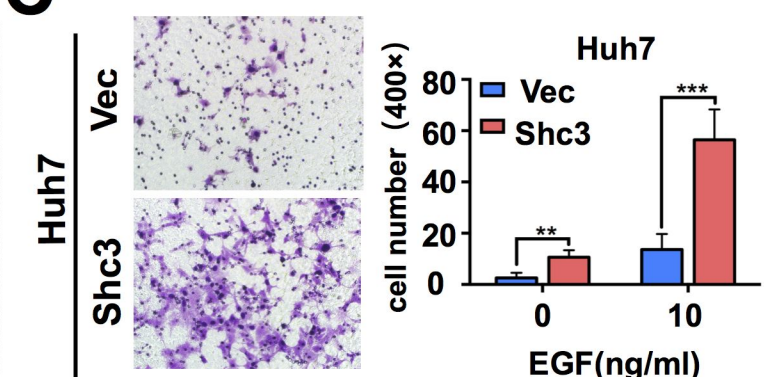
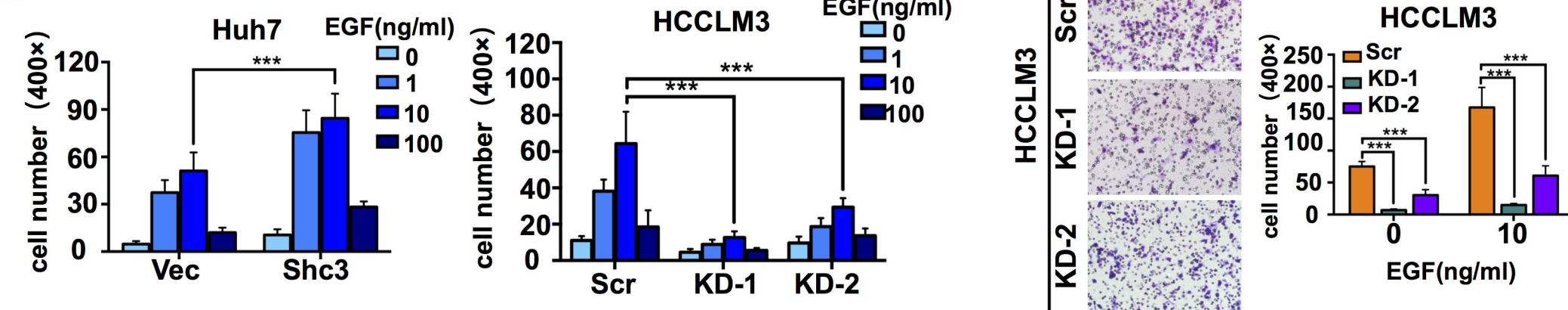
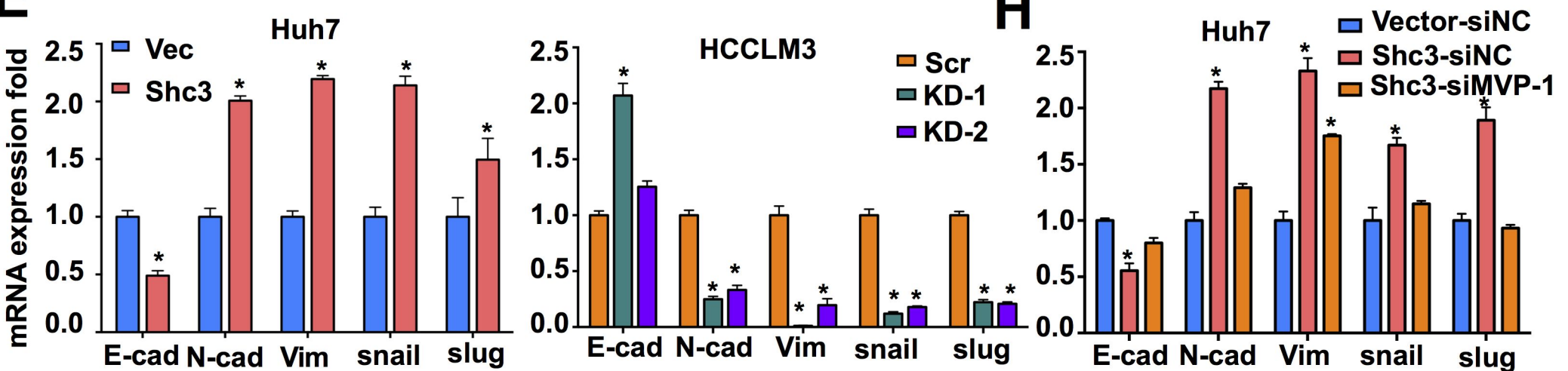
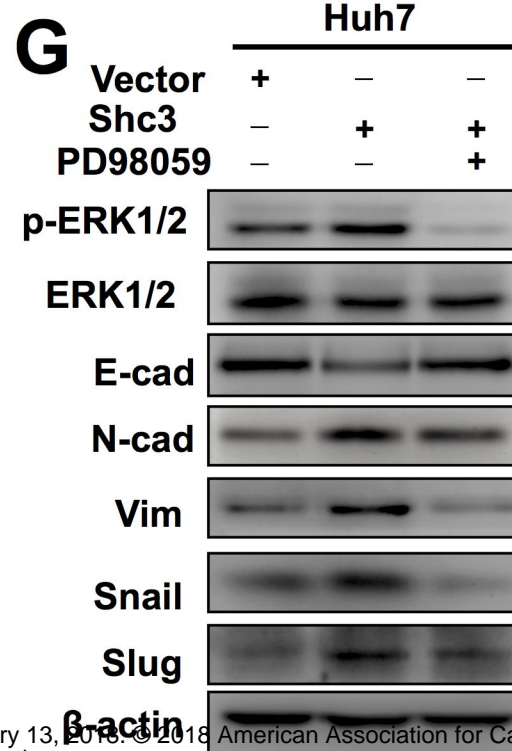
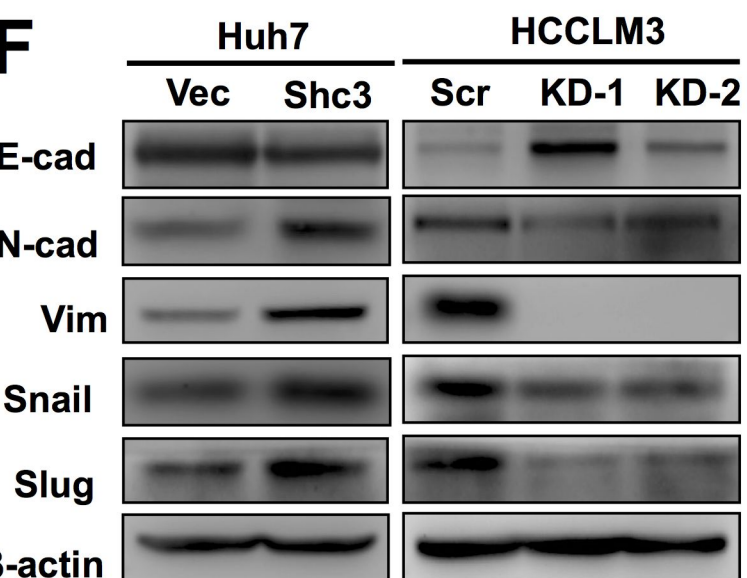
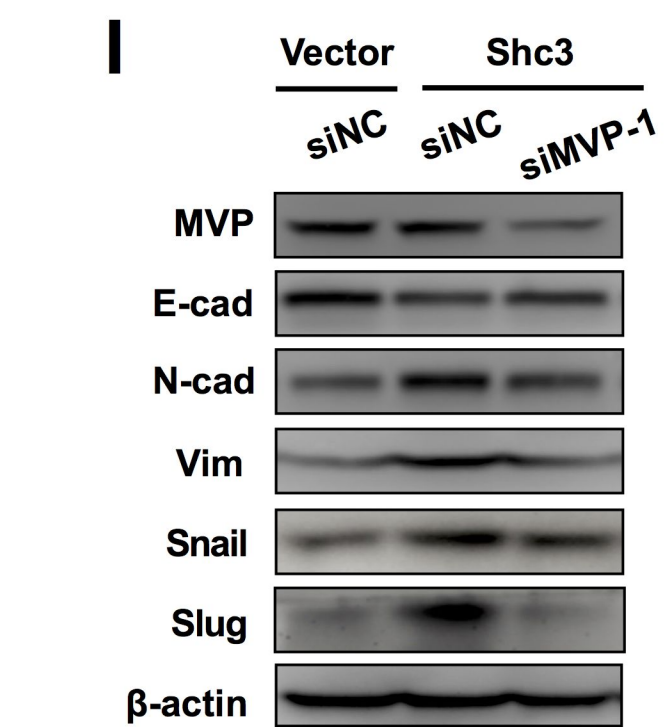
**C****D****E****F****G**

Fig.5

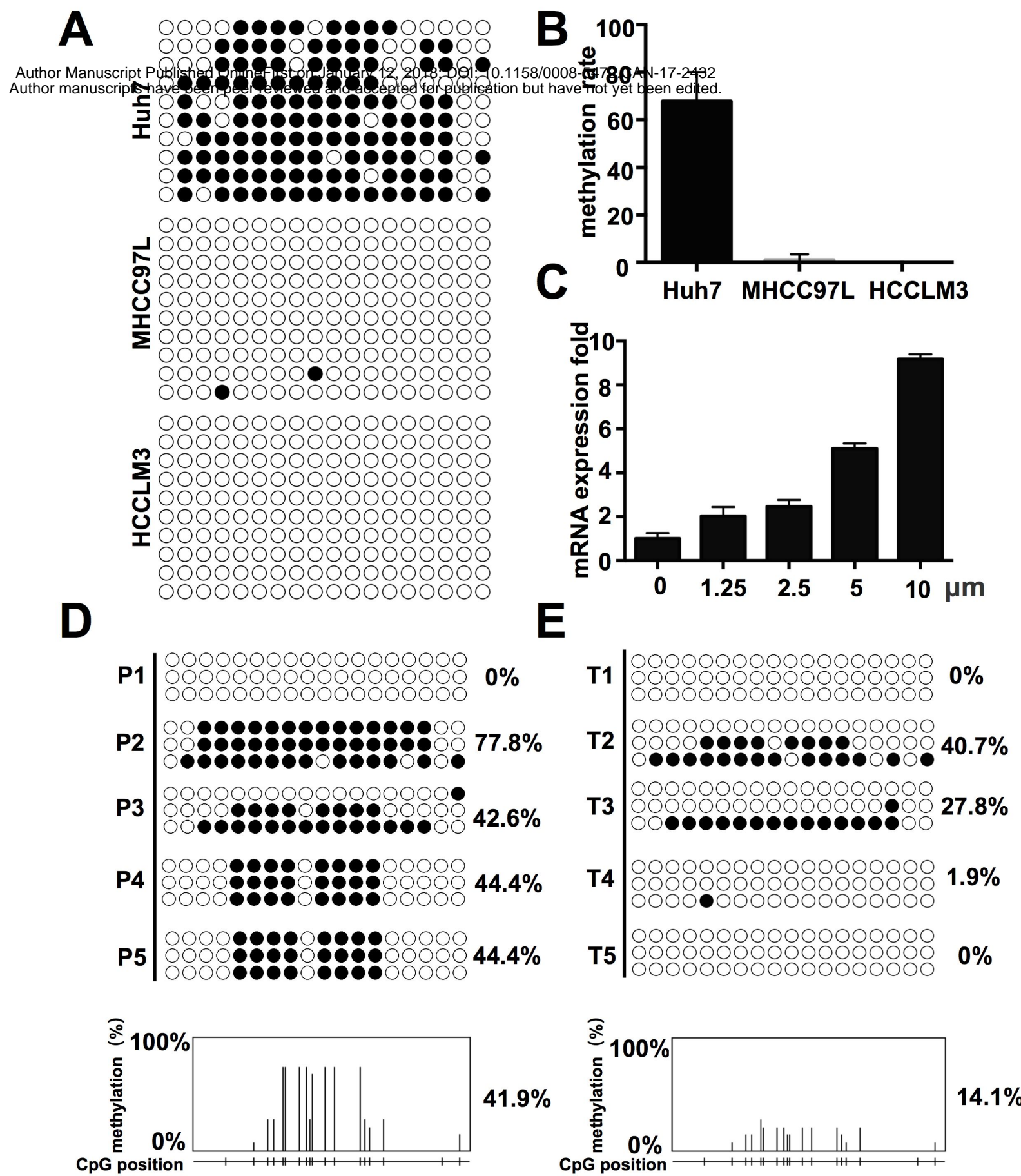


Fig.6

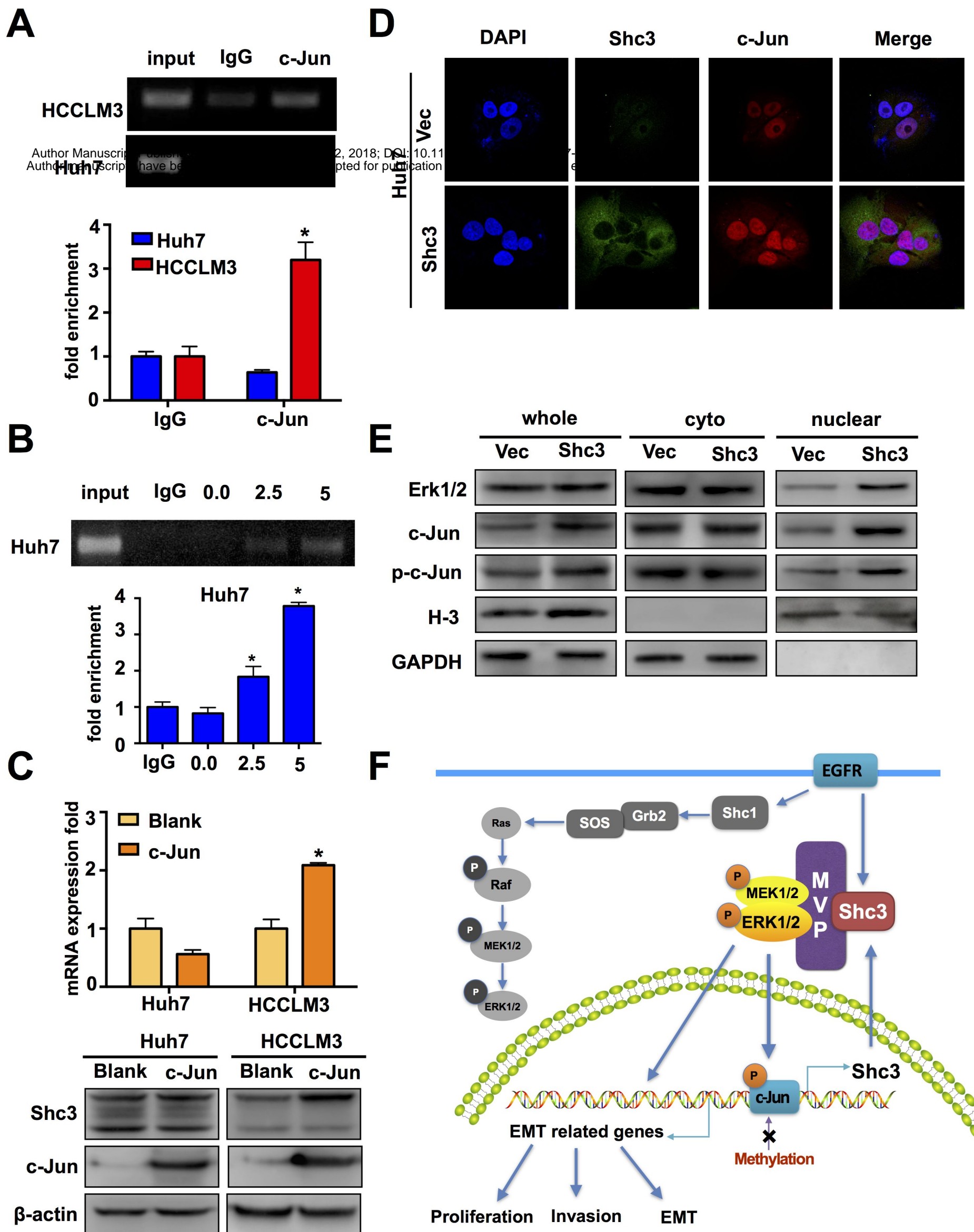
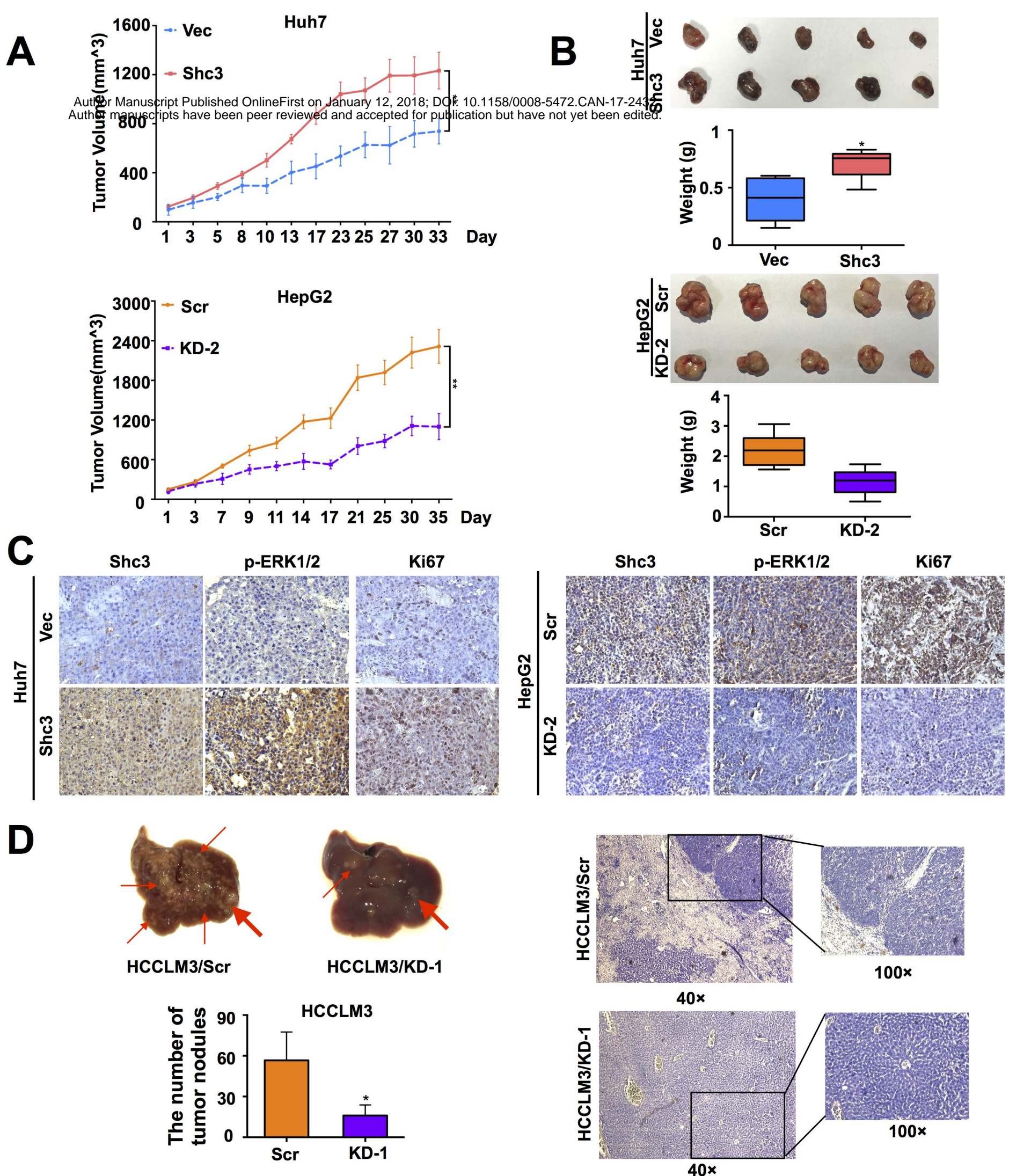


Fig.7



Cancer Research

The Journal of Cancer Research (1916–1930) | The American Journal of Cancer (1931–1940)

Demethylation-induced overexpression of Shc3 drives c-Raf-independent activation of MEK/ERK in HCC

Yun Liu, Xinran Zhang, Baicai Yang, et al.

Cancer Res Published OnlineFirst January 12, 2018.

Updated version	Access the most recent version of this article at: doi: 10.1158/0008-5472.CAN-17-2432
Supplementary Material	Access the most recent supplemental material at: http://cancerres.aacrjournals.org/content/suppl/2018/01/12/0008-5472.CAN-17-2432.DC1
Author Manuscript	Author manuscripts have been peer reviewed and accepted for publication but have not yet been edited.

E-mail alerts	Sign up to receive free email-alerts related to this article or journal.
Reprints and Subscriptions	To order reprints of this article or to subscribe to the journal, contact the AACR Publications Department at pubs@aacr.org .
Permissions	To request permission to re-use all or part of this article, use this link http://cancerres.aacrjournals.org/content/early/2018/01/12/0008-5472.CAN-17-2432 . Click on "Request Permissions" which will take you to the Copyright Clearance Center's (CCC) Rightslink site.